frontiers in Materials

ORIGINAL RESEARCH
published: 24 November 2020
doi: 10.3389/fmats.2020.601645

# Processing of $Sr^{2+}$ Containing Poly L-Lactic Acid-Based Hybrid Composites for Additive Manufacturing of Bone Scaffolds

*Priscila Melo[1], Raasti Naseem[2], Ilaria Corvaglia[1], Giorgia Montalbano[1], Carlotta Pontremoli[1], António Azevedo[3], Paulo Quadros[3], Piergiorgio Gentile[2], Ana Marina Ferreira[2], Kenneth Dalgarno[2], Chiara Vitale-Brovarone[1]* and Sonia Fiorilli[1]*

[1]Department of Applied Science and Technology, Politecnico di Torino, Torino, Italy, [2]School of Engineering, Newcastle University, Newcastle Upon Tyne, United Kingdom, [3]FLUIDINOVA, S.A., Maia, Portugal

OPEN ACCESS

**Edited by:**
*Kalisadhan Mukherjee, Pandit Deendayal Petroleum University, India*

**Reviewed by:**
*Ehsan Zamani, University of Nebraska-Lincoln, United States*
*Haizheng Tao, Wuhan University of Technology, China*

***Correspondence:**
*Chiara Vitale-Brovarone*
*chiara.vitale@polito.it*

**Specialty section:**
*This article was submitted to Ceramics and Glass, a section of the journal Frontiers in Materials*

**Received:** *01 September 2020*
**Accepted:** *30 October 2020*
**Published:** *24 November 2020*

**Citation:**
*Melo P, Naseem R, Corvaglia I, Montalbano G, Pontremoli C, Azevedo A, Quadros P, Gentile P, Ferreira AM, Dalgarno K, Vitale-Brovarone C and Fiorilli S (2020) Processing of $Sr^{2+}$ Containing Poly L-Lactic Acid-Based Hybrid Composites for Additive Manufacturing of Bone Scaffolds. Front. Mater. 7:601645. doi: 10.3389/fmats.2020.601645*

Biodegradable composite materials represent one of the major areas of investigation for bone tissue engineering due to their tuneable compositional and mechanical properties, which can potentially mimic those of bone and potentially avoid the removal of implants, mitigating the risks for the patient and reducing the overall clinical costs. In addition, the introduction of additive manufacturing technologies enables a strict control over the final morphological features of the scaffolds. In this scenario, the optimisation of 3D printable resorbable composites, made of biocompatible polymers and osteoinductive inorganic phases, offers the potential to produce a chemically and structurally biomimetic implant, which will resorb over time. The present work focuses on the development and process optimisation of two hybrid composite filaments, to be used as feedstock for the fused filament fabrication 3D printing process. A Poly L-lactic acid matrix was blended with either rod-like nano-hydroxyapatite (nano-HA) or nanoparticles of mesoporous bioactive glasses, both partially substituted with strontium ($Sr^{2+}$), due to the well-known pro-osteogenic effect of this ion. Both inorganic phases were incorporated into Poly L-lactic acid using an innovative combination of processes, obtaining a homogeneous distribution throughout the polymer whilst preserving their ability to release $Sr^{2+}$. The filament mechanical properties were not hindered after the incorporation of the inorganic phases, resulting in tensile strengths and moduli within the range of cancellous bone, 50 ± 10 MPa and 3 ± 1 GPa. Finally, the rheological characterization of the hybrid composites indicated a shear thinning behaviour, ideal for the processing with fused filament fabrication, proving the potential of these materials to be processed into 3D structures aiming bone regeneration.

**Keywords: mesoporous bioactive glasses, nanohydroxyapatite, fused filament fabrication, poly L-lactic acid matrix, hybrid composites, strontium release, bone scaffolds**

## INTRODUCTION

Bone is a dynamic tissue with the ability to self-renewal and heal, to maintain its stability and integrity (Lehmann et al., 2012; Kalani et al., 2019). Different pathologies such as osteoporosis hinder the balance between bone forming and resorption, leading to a decreased bone mass and consequently to a fracture. The numbers are constantly increasing, with an expected rise to 21 million by 2050 (Navarro et al., 2008; Pisani et al., 2016).

To overcome the limitations of the conventional treatments, tissue engineering (TE) has gained great interest, providing alternative strategies with the potential to produce immunologically tolerant artificial tissues and organs (Sachlos et al., 2003). TE uses a combination of biomaterials to produce 3D platforms - scaffolds - which can be implanted with or without cells, and functionalized with biologically active molecules, to provide an initial support for the native tissue, promoting its repair (Choudhury and Agrawal, 2012).

Scaffolds are usually produced with biodegradable materials, especially polymers for their tuneable properties and wide variety. Common polymers used in orthopaedics include poly-L-lactic acid (PLLA), polycaprolactone (PCL), and poly-L-glycolic acid (PLGA) (Kasuga et al., 2000; Alizadeh-Osgouei et al., 2019; Bharadwaz and Jayasuriya, 2020). PLLA is particularly attractive for its mechanical properties such as high tensile strength, low elongation, and elastic modulus comparable to bone (Middleton and Tipton, 2000; Narayanan et al., 2016). Additionally, this FDA approved polymer is biodegradable, biocompatible, and easily processed.

In terms of scaffold production, additive manufacturing (AM) technologies are appealing due to their ability to tailor structures in different orders of magnitude, using a wide range of materials with an increased design freedom (Melchels et al., 2012; Do et al., 2015). Allied to TE, AM techniques have the potential to create newly improved devices for bone repair (Bose et al., 2013). Recently, PLLA has been studied as a matrix in biocomposites, produced as feedstock for fused filament fabrication (FFF) of bone scaffolds, for critical size defects (Melo et al., 2019). During the printing process, the polymeric filament is fed through a temperature-controlled nozzle, where it melts, creating a melt pool, and then is extruded. The FFF technique is extremely cost-effective, and easily scalable for industrial production. Besides, FFF versatility in terms of employed materials and scalability makes it suitable for production of medical devices, especially in orthopaedics whose market is growing exponentially (Wang et al., 2017; Lee et al., 2019).

Considering the composite nature of bone, and with the aim to increase the affinity with the host tissue, bioceramics and bioglasses are a common choice as fillers in composites developed for bone TE (Du et al., 2018; Kumar et al., 2019). Nanohydroxyapatite (nano-HA) and mesoporous bioactive glasses (MBGs) are under focus for their biocompatibility, osteoinductive properties and bioactivity (Qi et al., 2018; Jiang et al., 2019). Furthermore, these inorganic phases can be tailored at a compositional level to deliver ions such as $Ag^{+}$, $Co^{2+}$, $Mg^{2+}$, $Sr^{2+}$, $Zn^{2+}$, $Ce^{3+/4+}$, $Ti^{4+}$, capable of promoting cell differentiation and osteogenesis, and/or exert an anti-inflammatory or antibacterial effect (Xie et al., 2012; Jiang et al., 2019). Strontium ($Sr^{2+}$), in particular, is well-known for the pro-osteogenic and anti-clastogenic abilities, stimulating bone regeneration in a compromised clinical context, such as osteoporosis (Gentleman et al., 2010; Kaygili et al., 2015; Querido et al., 2016).

Several approaches have been proposed to produce composites based on PLLA, PLGA or PCL as polymer matrix. In the literature, those polymers were mostly combined with HA in order to produce composite scaffolds with enhanced bioactive and osteoinductive abilities. For instance, PLGA-nano-HA composites were proved to be biocompatible, to display high cell viability *in vitro*, and to induce osteodifferentiation, the latter specifically imparted by the addition of nano-HA (Babilotte et al., 2021). Similar results were proved by Xiao et al. also for PLLA-HA hybrid systems, as the attachment, migration, and differentiation abilities of osteoblastic cells were found to be superior for the composite, if compared to plain analogue PLLA scaffold (Xiao et al., 2016). Liu et al. fabricated a strontium-containing PCL-HA composite scaffold for bone regeneration, which demonstrated facilitated cell proliferation and osteogenic differentiation along with an increased alkaline phosphatases activity (Liu et al., 2019). The previous examples underline the wide interest of the scientific community active in the field of bone regeneration, towards composite systems based on bioactive micro and nanoparticles in order to stimulate bone reforming ability.

In this respect, the aim of this study is to produce a bioactive hybrid composite with mechanical properties similar to native bone, able to provide a sustained release of osteogenic ions as a measure of treatment, and suitable for the design of scaffolds by means of AM technologies (Navarro et al., 2008).

PLLA is a well-known biomaterial and has been used extensively as matrix for composites containing HA, Bioglass and other bioceramics (Tripathi et al., 2010; Ramesh et al., 2018), however its merging with MBGs partially substituted with $Sr^{2+}$ has not been explored yet. In this work, two biocomposites were developed consisting in a PLLA matrix filled with nano-HA or MBGs, both containing $Sr^{2+}$ in their framework. Two distinct inorganic phases were chosen for their specific morphological characteristics and chemical composition. In particular, MBGs are characterized by high specific surface area (hundreds of $m^2/g$) and regular nanoporosity, which confer an excellent bioactive behaviour and allows the easy incorporation and release of active substances and/or ions (Yan et al., 2004; Wu and Chang, 2012). Nano-HA has the composition and morphology similar to bone apatite, conferring to the final hybrid formulations a higher level of biomimicry (Jiang et al., 2019; Kargozar et al., 2019). The morphology and composition of the employed inorganic phases is expected to affect aspects such as the ion release behaviour, which in turn influences the cells behaviour (Melo et al., 2019). Moreover, the surface features and the particle size likely influence the incorporation within the polymer matrix, consequently changing the final mechanical properties and degradation behaviour of the composite (Felfel et al., 2015; Valino et al., 2019).

Sr-substituted MBGs and nano-HA were synthesised and fully characterised, with focus on their morphology and $Sr^{2+}$ release kinetics, and then used to produce the hybrid composites, by soaking the polymer granules into a pre-formed aqueous-based paste dispersing the inorganic phases, a new methodology, unreported up to date. The resulting hybrid formulations were then easily inserted into an extruder and processed to produce a consistent filament.

The proposed approach is novel and allowed a straightforward incorporation of the inorganic phase into the polymeric matrix, without requiring toxic or flammable chemicals. Moreover, the extrusion of the obtained hybrid systems allowed the homogeneous dispersion of the inorganic phase within the PLLA matrix, avoiding excessive powder waste.

The extruded filaments were characterized in terms of morphological, mechanical, rheological properties, and ability to release $Sr^{2+}$ ions.

# MATERIALS AND METHODS

## Materials

PLLA granules (Purasorb PL 38) with average density of 1.24 g/$cm^3$ were obtained from Corbion (Purac Biomaterials). The $Sr^{2+}$ substituted nano-HA (HA_50%Sr) was obtained from FLUIDINOVA (Maia, Portugal). The MBGs were synthesised by the authors as described in next section.

## Synthesis of $Sr^{2+}$ Containing Mesoporous Bioactive Glasses

MBG nanoparticles containing strontium (MBG_SG_10%Sr) were synthesized via a sol-gel route (molar ratio Sr/Ca/Si = 10/5/85), based on a modified procedure reported by Wu et al. (2012). The protocol implies the preparation of two solutions that are later combined. In particular, solution A consisted of 25 ml of $NH_4OH$ (ammonium hydroxide solution, Sigma Aldrich, Milan, Italy) mixed with 140 ml of ethanol (EtOH). 12 g of cetilmethylammoium bromide (CTAB, ≥ 98%, Sigma Aldrich, Milan, Italy), were added to the solution and left to fully dissolve under stirring. Solution B was obtained by dissolving 9.4 g of tetraethyl orthosilicate (TEOS, Sigma Aldrich, Milan, Italy) in 50 ml of EtOH. Solution A was added to solution B and stirred for 20 min. Then 0.94 g of calcium nitrate tetrahydrate ($Ca(NO_3)_2{\cdot}4H_2O$, 99%, Sigma Aldrich, Milan, Italy) and 1.67 g of strontium nitrate ($Sr(NO_3)_2$, Sigma Aldrich, Milan, Italy) were added and stirred for 10 min. Finally, 4.7 g of TEOS were added and stirred for 5 h. The solution was centrifuged at 10,000 rpm for 3 min (Hermle Labortechnik Z326, Hermle LaborTechnik GmbH, Wehingen, Germany), and the precipitated powder was collected. This powder was washed three times with water, then once with 50% EtOH in water, and once with 100% EtOH. The final precipitate was dried overnight at 70°C. To remove the CTAB template, the powder was calcined at 600°C in air for 5 h (heating ramp 1°C/min, cooling ramp of 10°C/min, Carbolite 1300 CWF 15/5, Carbolite LTD, Hope Valley, UK).

## Production of the Composite Filaments

The production of the composite filaments was based on two successive steps. Firstly, aqueous suspensions containing the inorganic phases were made, then combined with PLLA granules to promote a homogeneous mixing of both materials. The obtained mixture was then extruded using a twin-screw extruder to produce the filaments (**Figure 1**).

In-house suspensions were produced by dispersing the powders of each inorganic phase in water at a 15 wt% concentration. The suspension was stirred for 20 min at room temperature at 300 rpm until completely homogeneous.

The incorporation of the inorganic phases into the polymer matrix was attained by contacting PLLA granules with the produced suspensions, containing a percentage of inorganic phase of 5 wt% for HA_50%Sr and 2 wt% for MBG_SG_10% Sr. The obtained soaked granules were distributed on weighing boats covered with pierced aluminium foil and placed under vacuum in a desiccator until complete water evaporation was achieved. Every 12 h the granules were removed from vacuum and manually stirred with a spatula to guarantee the homogeneous pellet coverage. To ensure the removal of the possible remaining moisture, the granules were dried overnight in an oven at 50°C.

A twin-screw extruder (Rondol Technology, France) was used to produce filaments. The composite granules were extruded, pelletized and re-extruded to promote the inorganic phase distribution. The temperatures defined for the first extrusion process were 125/240/240/220/180°C, from the hopper to the nozzle. The extruded material was inserted in a haul-off machine and pulled at 1.0 mm/s, for a feed speed of 15 ± 2 rpm and extrusion speed of 40 ± 10 rpm. The composite filaments were pelletized using a Rondol pelletizer and re-extruded with the following temperatures 125/200/200/180/160 C. A haul-off was set at 1.0 mm/s, for a hopper feed speed of 17 ± 1 rpm, and the extrusion speed of 19 ± 1 rpm. A single extrusion was applied to produce PLLA filaments, used as control.

## Characterization of MBG_SG_10%Sr and HA_50%Sr

The morphology of the MBG_SG_10%Sr and HA_50%Sr particles was studied with Field-Emission Scanning Electron Microscopy (FE-SEM) using a ZEISS MERLIN instrument (Oberkochen, Germany). For the analysis, 10 mg of powder were dispersed in 3 ml of isopropanol and sonicated using an ultrasonic bath (Digitec DT 103H, Bandelin) for 10 min to obtain a stable suspension. A drop of the suspension was deposited on a copper grid (3.05 mm Diam.200 MESH, TAAB, Aldermaston, Berks, UK), left at room temperature to evaporate the isopropanol and subsequently a chromium layer was sputtered to enhance the sample conductivity. The effective presence of $Sr^{2+}$ within the inorganic phase particles was investigated by means of Energy Dispersive X-Ray Spectroscopy (EDS), using the ZEISS MERLIN Instrument for the MBG_SG_10%Sr, and a scanning electron microscopy (SEM) (Desktop SEM Phenom XL, Phenom-World B.V., Netherlands) for the HA_50%Sr.

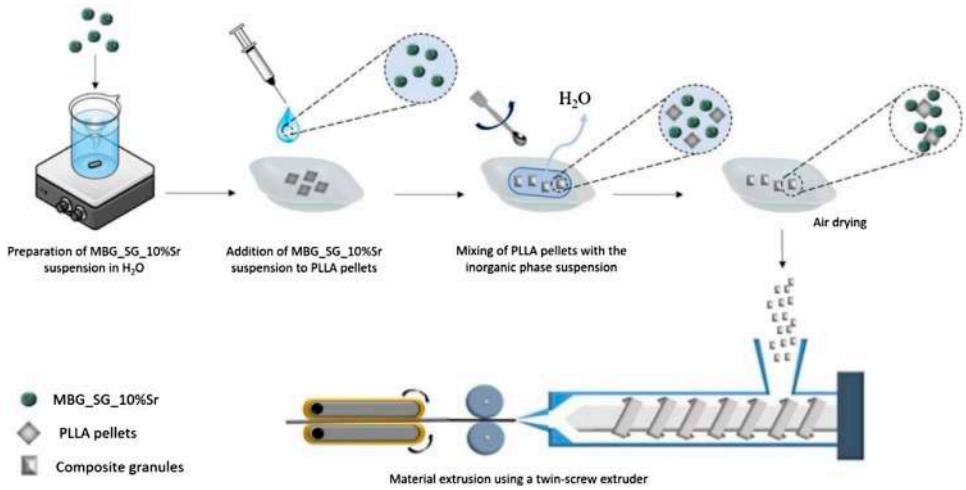


**FIGURE 1 |** Schematic representation of the process for the production of composite filaments containing MBG_SG_10%Sr (Melo, 2019). The same process was used for the filaments containing HA_50%Sr, except for the preparation of the related suspension (provided by FLUIDINOVA).

The particle's specific surface area (SSA) was measured by applying the Brunaeur, Emmett and Teller (BET) model, while the Density Functional Theory (DFT) method, using the NLDFT kernel of equilibrium isotherms, was applied to calculate the pore size distribution. Before the measurement, the sample was degassed at 150°C for 3 h. Nitrogen adsorption-desorption isotherms were measured at the temperature of -196°C (ASAP2020, Micromeritics ASAP 2020, Plus Physisorption, Norcross, GA, United States). X-ray diffraction (XRD) measurements (X'Pert PRO, PANanalytical, Almelo, Netherlands) were conducted only on HA_50%Sr samples exposing the powders to a CuKα radiation, imposing a current of 40 mA and a voltage of 40 mV. The analysed two theta (2θ) angles were between 10 and 80°, with a step size of 0.013 2θ degrees and a scan step time of 45 s. XRD spectrum analysis for phase identification was performed through the X'Pert HighScore software.

## Characterization of the Hybrid Composite Filaments

The hybrid composite filament characterization provided results about the inorganic phase distribution within the polymeric matrix as well as their mechanical and rheological properties.

To perform morphological analyses, filaments were cut into 4 ± 1 mm pieces and placed over an aluminium stub, covered with conductive carbon tape, to expose their cross-section. The samples were coated with a 7 nm chromium layer, to increase the sample conductivity, and the images were acquired using the Desktop SEM Phenom XL (Phenom-World B.V., Netherlands) at an accelerating voltage of 10 kV. The presence of strontium ions was detected by EDS.

To assess the tensile properties, filaments (n = 3) underwent tensile testing, using a Shimadzu Tester, equipped with a 1 kN load cell. The displacement-controlled tensile test used a speed of 30 mm/min, with termination of the test defined at 300 mm of material displacement, or when the rupture occurred. The gauge length for the samples was set as 300 mm.

Rheological analyses were conducted on a representative sample for each composite using a DHR-2 controlled stress rotational rheometer (TA Instruments, Waters, New Castle, DE, United States) equipped with an environmental test chamber to guarantee the strict control over the temperature during the tests. The analysis was done using a 25 mm parallel plate geometry, keeping a constant temperature of 220°C to mimic the value used during FFF processing of the filaments.

## $Sr^{2+}$ Ion Release From the Inorganic Phases and the Hybrid Filaments

The $Sr^{2+}$ release behaviour of both inorganic phases and the produced composite filaments was investigated with Inductively Coupled Plasma Atomic Emission Spectrometry Technique (ICP-AES) (ICP-MS, Thermo Scientific, ICAP Q).

For the powders, 5 mg were deposited in a glass vial and soaked in 20 ml of Tris HCl buffer (Tris(hydroxymethyl) aminomethane (Trizma) (Sigma Aldrich, Milan, Italy) 0.1 M, pH 7.4) (Fiorilli et al., 2018). The suspended powders were stored in an orbital shaker (Excella E24, Eppendorf) with an agitation rate of 150 rpm. The total duration of the test was 7 days for MBGs, and 21 days for nano-HA, with defined time points being 3 h, 24 h, 3 days and 7 days for both inorganic phases. Two time points were added for the nano-HA particles, 14 and 21 days, to match the important time points related to stem cell differentiation and mineralisation during bone repair (Einhorn and Gerstenfeld, 2015). These time points were not added to MBGs as the release of ions was already complete in the first week of assay, in analogy to the results obtained by the authors for similar systems (Fiorilli et al., 2018). At each time point the samples were centrifuged at 10,000 rpm for 5 min (Hermle Labortechnik Z326, Wehingen, Germany). Half of the supernatant was collected and then

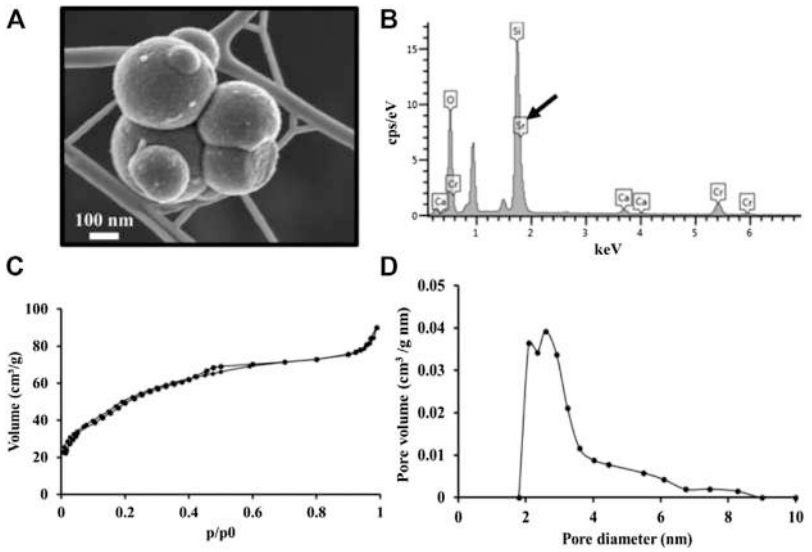


**FIGURE 2 | (A)** FE-SEM micrographs of MBG_SG_10%Sr nanoparticles; **(B)** EDS of MBG_SG_10%Sr showing peaks for Ca, Si, O and Sr (arrow) and Cr (from coating); **(C)** $N_2$ adsorption-desorption curves of MBG_SG_10%Sr; **(D)** DFT pore size distribution.

replaced by the same amount of fresh buffer solution. The release experiments were carried out in triplicate.

For the composite filaments, 0.3 g of material (n = 3) were immersed in 3 ml of Tris HCl buffer (same buffer as for the inorganic phases). The soaked fragments were stored in a static oven for 7 days. At each time point the medium was fully refreshed, being substituted with new media (Melo et al., 2019).

## Statistical Analysis

Experimental data are reported as mean ± standard deviation. Statistical differences between groups were analysed using one-way ANOVA with Tukey's pairwise *post-hoc* test. Statistical significance was represented as $^{*}p < 0.05$, $^{**}p < 0.01$, $^{***}p < 0.001$.

# RESULTS

## Characterization of MBG_SG_10%Sr and HA_50%Sr

Both inorganic phases were characterised, focusing on their morphology, composition, and presence of $Sr^{2+}$, in the desired amount. The MBG_SG_10%Sr particles appeared spherical with nanometric dimensions comprising between 200 and 300 nm (**Figure 2A**). The EDS analysis confirmed the glass composition based on calcium and silicon oxide as well as the presence of incorporated $Sr^{2+}$, as evidenced in **Figure 2B**.

Results from adsorption-desorption analysis on MBG_SG_10% Sr displayed a type IV isotherm, with a H2 hysteresis loop, typically associated with mesoporous materials containing both open and partially blocked mesopores (**Figure 2C**) (Thommes et al., 2015). The DFT method showed that pore size distribution is centred at 2–3 nm, with a maximum size of 6 nm (**Figure 2D**). The specific surface area and pore volume were calculated to be 190 $m^2/g$ and 0.13 $cm^3/g$, respectively.

Morphological analyses performed on HA_50%Sr using FE-SEM (**Figure 3A**) revealed a rod-like shape and the EDS analysis confirmed the effective incorporation of the $Sr^{2+}$ within the framework (**Figure 3B**). An estimation of the (Ca + Sr)/P ratio, the molar fraction of the ions constituting the material, demonstrated that the value obtained was comparable to stoichiometric ratio in non-substituted hydroxyapatite (Kalita et al., 2007).The XRD peaks of HA_50%Sr (**Figure 3C**) were in the characteristic positions of HA (002, 211, 112, 300, 222 and 213 peaks) as confirmed be the values registered in the ICDD database.

The ion release test from the MBGs, conducted with Tris-HCl medium, displayed a burst release after 3 h, approximately 60% of the incorporated ions. This was followed by a plateau, where the release continued until day 7, and 95% of the $Sr^{2+}$ ions left the network (**Figure 4A**). The ion release test from nano-HA revealed that after 1 day, 20% of the incorporated $Sr^{2+}$ was released from the sample (**Figure 4B**). The release kinetics from those particles appeared sustained as, after 21 days, 45% of the incorporated ions was measured into the soaking medium.

## Characterization of the Extruded Composite Filaments

The extruded composite filaments were characterised regarding the inorganic phase distribution into the polymer matrix, and to assess its influence over the tensile and rheological properties of the extruded material.

The composite filaments were extruded obtaining a constant diameter (1.6 ± 0.1 mm), with a smooth surface. The

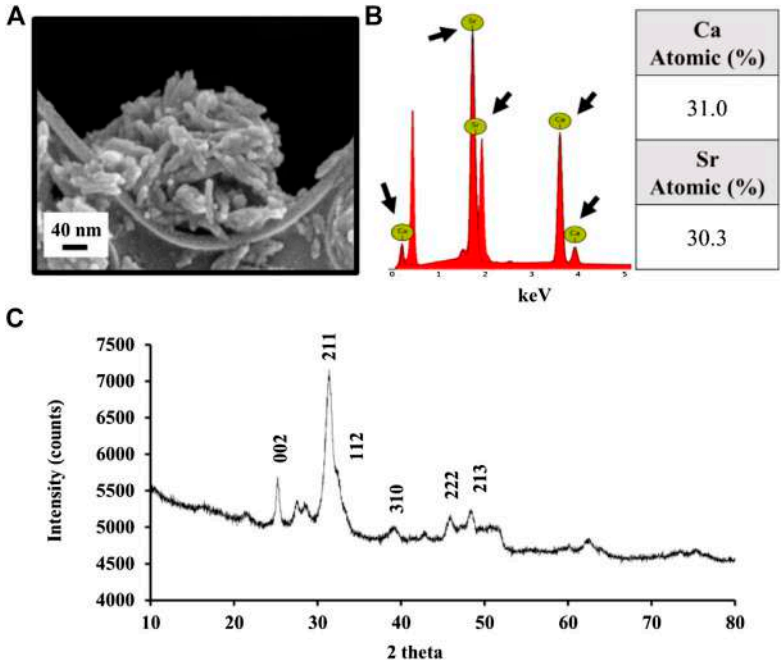


**FIGURE 3 | (A)** FE-SEM micrographs of HA_50%Sr nanoparticles.; **(B)** EDS of HA_50%Sr marking peaks for Ca and Sr (arrows) with table indicating the atomic percentage estimated for each element; **(C)** XRD pattern of HA_50%Sr.

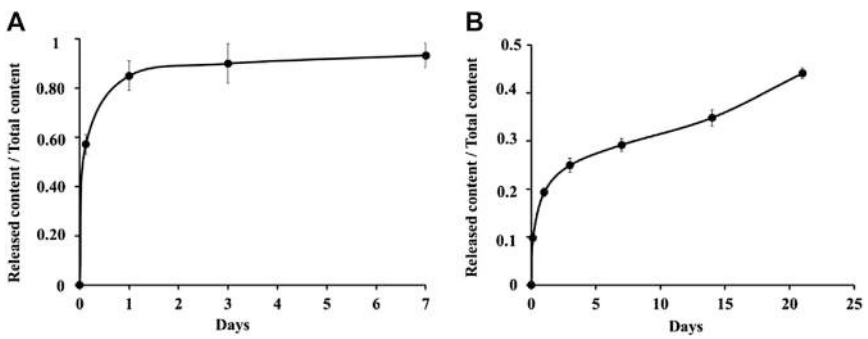


**FIGURE 4 |** Ion release profile of inorganic phases. **(A)** MBG_SG_10%Sr nanoparticles; **(B)** HA_50%Sr. The results are expressed as mean ± SD.

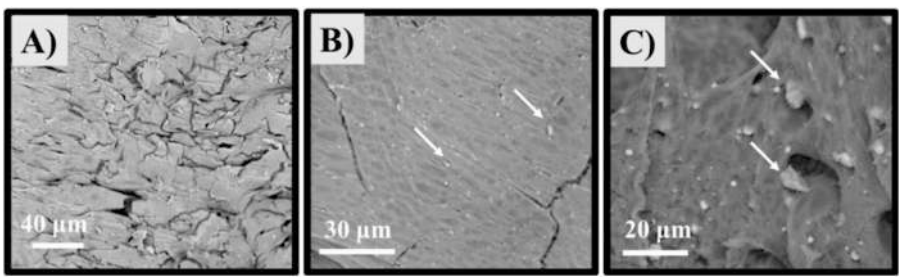


**FIGURE 5 |** SEM micrographs of produced filaments cross-section. A) PLLA, B) PLLA_MBG_SG_10%Sr and C) PLLA_HA_50%Sr. The white arrows indicate the inorganic phases embedded into the PLLA matrix.

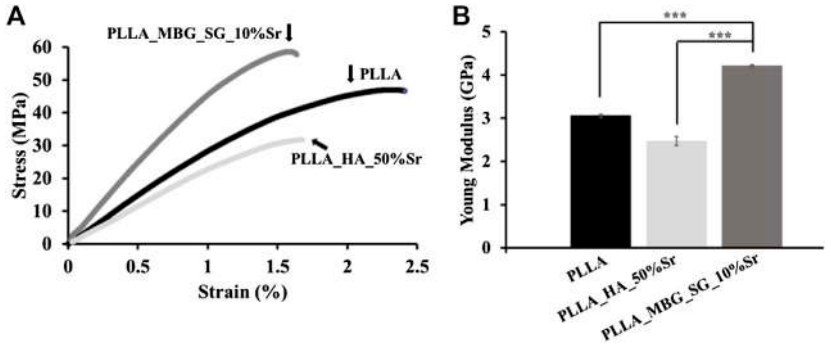


**FIGURE 6 |** Tensile properties of the extruded filaments. **(A)** Stress-strain curves; **(B)** Young Modulus. The results are expressed as mean ± SD, ***$p < 0.001$.

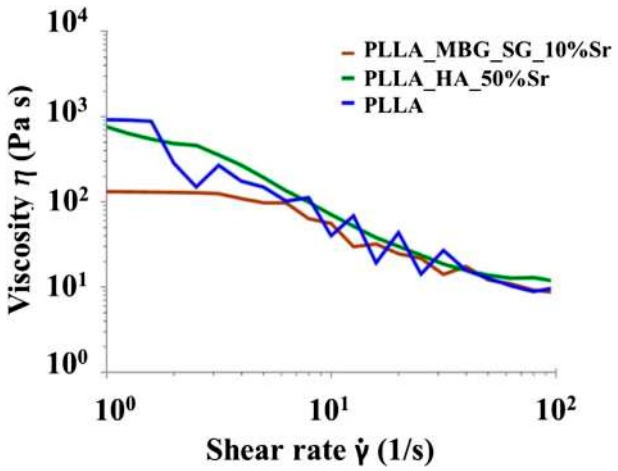


**FIGURE 7 |** Shear thinning behaviour of PLLA, PLLA_MBG_SG_10%Sr and PLLA_HA_50%Sr filaments at 220°C.

**TABLE 1 |** Values of ultimate tensile strength and Young Modulus for PLLA and composite samples

| Sample | Ultimate tensile strength in MPa (Mean ± SD) | Young Modulus in GPa (Mean ± SD) |
|---|---|---|
| PLLA | 47.1 ± 5.8 | 3.10 ± 0.04 |
| PLLA_MBG_SG_10%Sr | 58.8 ± 8.8 | 4.20 ± 0.02 |
| PLLA_HA_50%Sr | 35.6 ± 3.4 | 2.50 ± 0.10 |

morphological analysis of the filaments cross-section (**Figure 5**) confirmed the homogeneous incorporation of both inorganic phases within the polymer matrix without showing any significant agglomerate (**Figures 5B, 5C**). The presence of strontium on the indicated particles was confirmed with EDS analysis (**Supplementary Figure 1**).

**Figure 6A** displays representative curves from tensile testing. The ultimate tensile strength of the PLLA_MBG_SG_10%Sr composite was slightly increased when compared to the pure PLLA sample. On the contrary, the PLLA_HA_50%Sr composite displayed a reduction in the mechanical performance. The strain was greater for pure PLLA samples when compared with the composite materials, which were more brittle. The Young Modulus (**Figure 6B**), in analogy with the tensile strength, increased for PLLA_MBG_SG_10% Sr and decreased for PLLA_HA_50%Sr, when compared to pure PLLA.

The viscoelastic properties of PLLA and composite filaments were investigated at 220°C, the temperature previously used for FFF of PLLA filaments. Using a frequency sweep test, the variation of the storage modulus (G') and loss modulus (G'') with increasing angular frequency (from $10^0$ to $10^3$ rad/s) were investigated (**Supplementary Figure 2**). The values obtained from the frequency sweep analysis were used to obtain the material flow ramp, by applying the Cox-Merz equation (Bair et al., 2014), where the variation of the material viscosity was obtained for increasing shear rates ($10^0$–$10^2$ $s^{-1}$) (**Figure 7**).

The frequency sweep tests confirmed the viscous behaviour and thus the liquid-state of the material at 220°C for all the analysed samples, where G'' presented higher values compared to the G' at lower frequencies (**Supplementary Table 1**). In detail, G' and G'' for pure PLLA at low frequencies were measured to be higher than the values shown by the composites. At increased frequencies, storage modulus increased and overcame the loss modulus, reversing the tendency, and indicating the solid-like behaviour of the materials.

The potential printability of the filaments was tested observing the correspondent flow ramps (**Figure 7**). All the materials proved to be shear-thinning as a decrease of the viscosity values was observed with increasing shear rates (Barnes, 2003). At lower shear rates, PLLA displayed the highest value of viscosity, about 922 Pa s while the PLLA_MBG_SG_10%Sr samples showed the lowest value, about 132 Pa s. At the highest shear rates (100 $s^{-1}$), all materials showed very low values of viscosity (between 8 and 12 Pa s), confirming the shear thinning behaviour.

The ICP analysis conducted on the extracts of the composite filaments are reported in **Table 3**, which shows the ability to

**TABLE 2 |** Values of viscosity at a shear rate of 1 and 100 $s^{-1}$ for PLLA and composite samples

| Sample | Viscosity (Pa s) at 1 $s^{-1}$ shear rate | Viscosity (Pa s) at 100 $s^{-1}$ shear rate |
|---|---|---|
| PLLA | 922 | 10 |
| PLLA_MBG_SG_10%Sr | 132 | 8 |
| PLLA_HA_50%Sr | 764 | 12 |

**TABLE 3 |** $Sr^{2+}$ ion released from the composite filaments after 7 days of soaking

| Hybrid composite | $Sr^{2+}$ released in ppb (Mean ± SD) |
|---|---|
| PLLA_MBG_SG_10%Sr | 265 ± 23 |
| PLLA_HA_50%Sr | 489 ± 36 |

release of $Sr^{2+}$ after 7 days, with a slightly higher concentration detected for PLLA_HA_50%Sr.

# DISCUSSION

## $Sr^{2+}$ containing Inorganic Phases: Morphology and Structural Features

The synthesised MBGs had dimensions and structural characteristics in accordance with other studies, demonstrating that the incorporation of Ca-substituting ions within the framework did not greatly affect their dimensions (Erol and Boccaccini, 2011; Kaur et al., 2014; Neščáková et al., 2019) and morphology (Pontiroli et al., 2017). The pore dimensions, ranging from 2 to 6 nm, can be ascribed according to Yan et al. (2005), to one-dimensional channels developed within the structure (smaller size) and to the occurrence of the interconnected meso-channels (larger size). As far as other structural parameters, specific surface area and pore volume were smaller if compared to other particles developed according to the same synthesis process, but without the addition of $Sr^{2+}$ precursor. Previous studies on the incorporation of $Sr^{2+}$ (4% molar) within the MBG framework showed the same effect, therefore justifying the observed reduction in specific surface area and pore volume (Fiorilli et al., 2018). In this work, the amount of $Sr^{2+}$ was further incremented to 10% molar, aiming to enhance the final released concentration of this ion from the inorganic phases, when embedded into the PLLA polymeric matrix.

For $Sr^{2+}$-substituted nano-HA, the morphology appears rod-like with crystals measuring 50 ± 10 nm long and 15 ± 1 nm wide, close to that of biological apatite, whose dimensions are known to be about 40–60 nm long, and 20 nm wide (Kalita et al., 2007). The (Ca + Sr)/P ratio 1.65 ± 0.13 was comparable to that of non-substituted HA, known to be 1.67, showing that the $Sr^{2+}$ did not affect the overall stoichiometry, which is a key compositional and structural parameter (Kalita et al., 2007). Moreover, the XRD patterns confirmed that the degree of crystallinity was also similar to bone apatite, despite the $Sr^{2+}$ inclusion (Ofudje et al., 2019), however with a slight shift in the peaks position towards higher two theta and change in intensity compared to non-substituted HA, due to slight modification of the unit cell parameters upon $Sr^{2+}$ incorporation (Ofudje et al., 2019). The peak broadening could be related to a decrease of primary crystallite size (Ofudje et al., 2019), derived from the heterogeneity of the partially substituted sample. The decrease in crystallinity is expected to enhance the ion release from nano-HA being more prone to dissolution, and this feature is essential to influence the cell response throughout the healing process. If the dissolution behaviour is enhanced the concentration of ions exerting a biological effect is higher, and consequently the cell response is expected to be amplified, promoting bone repair (Yilmaz et al., 2019).

## The Extrusion Process and Final Properties of the Hybrid Filaments

The temperatures and parameters previously listed, for the first extrusion process, were already optimized for pure PLLA filaments, to attain a diameter of 1.7–1.75 mm, compatible with most of FFF printers (Gilmer et al., 2018; Nienhaus et al., 2019). As the material was not sufficiently homogenous upon a first extrusion, a second extrusion process was introduced for the composites.

The higher temperatures in the first extrusion reduce the viscosity and allow for better mixing to promote dispersion. An appropriate dispersion of the inorganic phase within the matrix is key to ensure that the mechanical properties are homogeneous throughout the filament. Furthermore, no voids were observed at the polymer-particle interface, which is particularly important as the presence of these voids would be detrimental to the overall mechanical performance of the material (Liu et al., 2014). Moreover, the selected particle size (below 5 μm) was also reported to be beneficial for the mechanical properties of composites, as it promotes the homogenous distribution and the adherence of the inorganic phase (Damadzadeh et al., 2010). The lower temperatures in the second extrusion give better dimensional control. Most FFF printers available on the market require an average 1.75 mm, but depending on the model and level of customisation, they can work with a higher/smaller range of filament sizes, within limits, also because commercial filaments also present size irregularities (Gilmer et al., 2018; Nienhaus et al., 2019). That a consistent filament can be produced using these materials is the key processing observation, as modifications to the die and haul-off would allow a 1.75 mm average diameter to be achieved. The distribution of the inorganic phases within the composite matrix was confirmed by SEM. These results were achieved using a simple solvent free process which allowed adhesion of the inorganic powders to the surface of polymer pellets. Subsequently this allowed a combination of the polymer and inorganic materials with twin-screw extrusion. Similar processes combing inorganic phases and polymers, that are solvent free, have been reported before (Melo et al., 2019), based on the direct mazing of the inorganic particles in a metal mode, however, the

immersion polymer granules in a paste containing the inorganic phase, for this unique purpose, was not reported up to date.

The homogeneous distribution of the inorganic phase within the polymeric matrix is essential for isotropic mechanical properties. From the results of the tensile test, it can be observed that incorporation of the MBGs to the polymer matrix increased the mechanical properties of the extruded filaments, in comparison to pure PLLA. The PLLA_HA_50%Sr composite on the contrary depicted a marked decrease in the mechanical properties, which could be attributed to the particle shape and surface, rod-like and with a low visible roughness, which hinders the adherence between polymer chains and embedded particles. Previous studies report the same effect when an inorganic phase could not adhere to the polymer, therefore causing an early failure at the polymer-inclusion interface (Fu et al., 2017). Instead, the MBGs particles are spherical and possess a high surface area, allowing for a higher degree of interface between materials, therefore a stronger integration within the matrix. The increase in Young's modulus for the composite formulations followed the same tendency, which is also reported in the literature, demonstrating that the inorganic phase introduction can reinforce the matrix (Bonfield et al., 1981; Shikinami and Okuno, 2001).

The composite filaments were further characterised for their rheological behaviour, highlighting the variation of the viscoelastic character as a function of temperature and stress conditions. Since the filaments are meant to be processed with FFF, it was fundamental to characterize their behaviour at 220°C, the common temperature used for the PLLA. Under this temperature, the reduced values of G' and G" registered for PLLA composites, compared to PLLA alone, can be associated with the material processing involving two extrusions. Indeed, the two-steps extrusion inserts a second step of thermal degradation, which is expected to cause a reduction of the polymer molecular weight, leading to a decrease in the length of the polymeric chains, consequently affecting the structural integrity of the material under stress (Wang, 2003). The frequency sweep test performed on the different filaments allowed to obtain the material viscosity when subjected to increasing shear rates, providing highly useful indications for the definition of the FFF processing parameters. Since the nozzle diameter is typically smaller than the filament (0.25 mm nozzle for a 1.75 mm filament), the material is subjected to an increased shear rate. This is key to avoid excessive extrusion and to attain increased precision in the deposition (Gibson et al., 2010), meaning a shear thinning behaviour is desirable for an optimal extrusion (Ramanath et al., 2008; Anderegg et al., 2019). This was successfully registered for both pure PLLA and composite filaments, meaning that all tested materials are suitable for FFF printing. Using FFF printing, the next step of this study will be to produce scaffolds using the designed hybrid formulations and assess them in terms of biocompatibility. According to existing literature, all materials combined to produce the hybrid formulations have already proven to be fully biocompatible (Kalita et al., 2007; Yoon et al., 2017; Elmowafy et al., 2019). In addition, the used PLLA, an FDA-approved copolymer, has been used extensively as a matrix for other biocomposites, which all demonstrated to be biocompatible when seeded with human mesenchymal stromal cells (Melo et al., 2019). PLLA/HA biocomposites are widely known, and several commercial products can be found (e.g. OSTEOTRANS MX range). Other composites have also been created using different percentages of HA (surface modified and with different ionic composition) in PLLA matrices, all reporting enhanced cell growth and proliferation (Akindoyo et al., 2019; Backes et al., 2020). The incorporation of MBGs in thermoplastic matrices is not as common as for HA, but studies involving their mixing with PCL (Yun et al., 2011) and Poly(3-hydroxybutyrate-co-3-hydroxyhexanoate) (PHBHHx) (Zhao et al., 2014) report successful cell growth and proliferation. Moreover, based on previous assessments (Baino and Fiume, 2020; Kermani et al., 2020), the MBGs are characterized not only by an excellent biocompatibility, but also by an osteogenic potential, desirable in bone healing devices.

## $Sr^{2+}$ Release From Inorganic Phases and Extruded Hybrid Filaments

The ion release kinetics were assessed for both inorganic phases and the hybrid composite filaments, in order to evaluate the ability of nano-HA and MBGs to deliver the therapeutic ions, alone and when embedded in the polymer matrix. As already observed by the authors, for MBGs containing $Sr^{2+}$ at lower amounts (4% mol.) a burst ion release is observed in the first 2 h of soaking. Fast ion release, commonly reported for substituted MBGs is due to the high surface area and accessible internal pore volume, which greatly enhances the surface ion-exchange reactions especially for framework ions exposed at the pore entrances. At 7 days, the majority (95%) of $Sr^{2+}$ content was released from the silica network. A small percentage remained within the mesoporous structure, probably due to a partial dissolution and reprecipitation of MBGs framework at the mesopore entrance, causing the inaccessibility to the soaking medium.

At variance, the release curve obtained for $Sr^{2+}$-substituted nano-HA showed a controlled and prolonged ion delivery associated with the material dissolution. The solubility of nano-HA particles is expected to be affected by the inclusion of $Sr^{2+}$ into the lattice, resulting higher if compared to non-substituted HA, as previously reported for other substituting ions (Zhu et al., 2018).

The release test on the composite filaments showed that both nano-HA and MBGs particles were able to deliver $Sr^{2+}$ ions, evidencing their accessibility to the soaking medium although incorporated into PLLA. At the considered time point (7 days), the ion release is supposed to originate from the particles exposed at the surface and cross sections of the filaments. The ion leaching could also be promoted, up to a certain degree, by the infiltration of the soaking medium into the polymeric matrix, enabling the contact with fully embedded particles. However, this contribution is considered minimal at the selected time point, as the diffusion of soaking media throughout the polymer structure is mostly controlled by the hydrolytic degradation of PLLA, which is expected to initiate within 8 weeks, under physiological

conditions (Melo et al., 2019; Melo et al., 2019). The observed released amount of $Sr^{2+}$ proved to be very similar for the two investigated filaments, despite what is shown in **Figure 4A**, where the release kinetics of $Sr^{2+}$ from MBGs alone appears much faster than from nano-HA (**Figure 4B**). On the other hand, the amount of MBGs loaded (2 wt%) into the extruded filaments was lower compared to the nano-HA which was 5 wt% and this difference could account for a higher exposure of the latter, compared to MBG particles. Furthermore, it is worth noting that, if fully embedded into the PLLA matrix the internal surface area associated to the mesoporous structure of MBGs would be inaccessible, thus not available for ion-exchange reactions with the soaking medium. Further degradation tests on the extruded composite filaments are required and will be the subject of future studies in order to investigate and compare the release behaviour over a longer period of time.

Considering the existing studies on similar composite systems, the final biocomposites developed in this work are expected to allow the processing of a fully biocompatible structure. Despite the high availability of composites containing PLLA and HA (also other bioceramics), up to date no reports are found on composites containing $Sr^{2+}$ substituted HA or MBGs. Being able to tune the inorganic phase composition is an additional advantage as it can confer the scaffolds other beneficial features. In the case of the composites developed in this study, this reflects on the osteogenic and anticlastogenic potential of $Sr^{2+}$, present in both MBGs and HA, making the material ideal for the treatment of osteoporosis-related issues, where bone density is low and bone resorption is high (Fiorilli et al., 2018).

## CONCLUSIONS

The need for improved devices targeting pathologies such as osteoporosis has created an increasing interest for additive manufactured scaffolds, which are capable of mimicking bone composition and mechanical properties.

In this context, this work aims to optimize a hybrid formulation for AM of advanced bone scaffolds, through the combination of a medical graded polymer, PLLA, with inorganic phases, MBGs and nano-HA, able to promote bone regeneration by stimulating osteogenesis. To enhance this osteogenic potential, and to provide an anticlastogenic effect, both MBGs and nano-HA were substituted with $Sr^{2+}$, and the obtained particles combined with PLLA. In particular, the authors aimed to develop and optimize new, overall green, approach to produce composite filaments using a combination of manual mixing and solvent free twin-screw extrusion. Composite filaments were successfully produced, showed a satisfactory dispersion of the inorganic phase and a diameter comparable to the commercially available filaments, proving their potential for FFF printing. Both inorganic phases alone when in contact with media mimicking the physiological conditions were able to release $Sr^{2+}$, although with very dissimilar kinetics. The composite extruded filaments also proved to release $Sr^{2+}$ within 7 days, meaning that the inorganic particles, although combined with PLLA matrix preserve their ability to deliver ions associated with pro-osteogenic and anti-clastogenic effects.

The characterisation of the elastic modulus, strength and viscosity showed that the composite materials had broadly similar mechanical and fluid properties as the pure PLLA, with the MBG-based composite showing higher strength. Furthermore, PLLA and composite filaments showed a shear thinning rheological response, highlighting their suitability for FFF printing.

The proposed composite manufacturing protocol could also be applied to other thermoplastics and inorganic phases, which further extends the potential of this method to create bespoke structures, tuned from the material composition level. Being an accessible methodology, easily scalable, it opens the possibility to use a myriad of material combinations, further extending its application range, to not only other medical devices, but also different industries.

## DATA AVAILABILITY STATEMENT

The datasets presented in this study can be found in online repositories. The names of the repository/repositories and accession number(s) can be found below: 10.5281/zenodo.4155423.

## AUTHOR CONTRIBUTIONS

For this research paper, CV-B, KD and SF formulated the research ideas. PM, RN and IC developed the manufacturing method, contributed to the characterization, and interpreted the results under the supervision of CV-B, SF, KD, PG and AF. GM conducted the overall rheological characterization and related data interpretation. CP synthesized and characterized MBG samples. AA and PQ developed the formulations and protocols to produce the nano-HA with 50% Sr2+ substitution. AA produced the nano-HA material. PM, RN, IC and GM have written the manuscript and all other authors revised the manuscript and contributed to the discussion of the results. SF, CV-B and KD have reviewed and edited the manuscript.

## FUNDING

This project has received funding from the European Union's Horizon 2020 research and innovation program under grant agreement No. 814410.

## SUPPLEMENTARY MATERIAL

The Supplementary Material for this article can be found online at: https://www.frontiersin.org/articles/10.3389/fmats.2020.601645/full#supplementary-material.

## REFERENCES


Akindoyo, J. O., Beg, M. D. H., Ghazali, S., Alam, A. K. M. M., Heim, H. P., and Feldmann, M. (2019). Synergized poly(lactic acid)–hydroxyapatite composites: biocompatibility study. *J. Appl. Polym. Sci.* 136, 1–10. doi:10.1002/app.47400

Alizadeh-Osgouei, M., Li, Y., and Wen, C. (2019). A comprehensive review of biodegradable synthetic polymer-ceramic composites and their manufacture for biomedical applications. *Bioact. Mater.* 4, 22–36. doi:10.1016/j.bioactmat.2018.11.003

Anderegg, D. A., Bryant, H. A., Ruffin, D. C., Skrip, S. M., Fallon, J. J., Gilmer, E. L., et al. (2019). *In-situ* monitoring of polymer flow temperature and pressure in extrusion based additive manufacturing. *Addit. Manuf.* 26, 76–83. doi:10.1016/j.addma.2019.01.002

Babilotte, J., Martin, B., Guduric, V., Bareille, R., Agniel, R., Roques, S., et al. (2020). Development and characterization of a PLGA-HA composite material to fabricate 3D-printed scaffolds for bone tissue engineering. *Mater. Sci. Eng. C* 118, 111334. doi:10.1016/j.msec.2020.111334

Backes, E. H., Pires, L. D. N., Beatrice, C. A. G., Costa, L. C., Passador, F. R., and Pessan, L. A. (2020). Fabrication of biocompatible composites of poly(lactic acid)/hydroxyapatite envisioning medical applications. *Polym. Eng. Sci.* 60, 636–644. doi:10.1002/pen.25322

Baino, F., and Fiume, E. 3D printing of hierarchical scaffolds based on mesoporous bioactive glasses (MBGs)-Fundamentals and applications. (2020). *Materials (Basel)* 13(7):1688. doi:10.3390/ma13071688

Bair, S., Yamaguchi, T., Brouwer, L., Schwarze, H., Vergne, P., and Poll, G. (2014). Oscillatory and steady shear viscosity: the Cox-Merz rule, superposition, and application to EHL friction. *Tribol. Int.* 79, 126–131. doi:10.1016/j.triboint.2014.06.001

Barnes, H. A. A review of the rheology of filled viscoelastic systems. (2003). *Rheol. Rev.* 2003, 1–36. doi:10.1081/ASR-120017479

Bharadwaz, A., and Jayasuriya, A. C. (2020). Recent trends in the application of widely used natural and synthetic polymer nanocomposites in bone tissue regeneration. *Mater. Sci. Eng. C* 110, 110698. doi:10.1016/j.msec.2020.110698

Bonfield, W., Grynpas, M. D., Tully, A. E., Bowman, J., and Abram, J. (1981). Hydroxyapatite reinforced polyethylene - a mechanically compatible implant material for bone replacement. *Biomaterials* 2, 185–186. doi:10.1016/0142-9612(81)90050-8

Bose, S., Vahabzadeh, S., and Bandyopadhyay, A. (2013). Bone tissue engineering using 3D printing. *Mater. Today* 16, 496–504. doi:10.1016/j.mattod.2013.11.017

Choudhury, P., and Agrawal, D. C. (2012). Hydroxyapatite (HA)coatings for biomaterials. In *Nanomedicine*. Editor T. J. Webster (Philadelphia, PA: Woodhead Publishing), 84–127.

Damadzadeh, B., Jabari, H., Skrifvars, M., Airola, K., Moritz, N., and Vallittu, P. K. (2010). Effect of ceramic filler content on the mechanical and thermal behaviour of poly-l-lactic acid and poly-l-lactic-co-glycolic acid composites for medical applications. *J. Mater. Sci. Mater. Med.* 21, 2523–2531. doi:10.1007/s10856-010-4110-9

Do, A. V., Khorsand, B., Geary, S. M., and Salem, A. K. (2015). 3D printing of scaffolds for tissue regeneration applications. *Adv. Healthc. Mater.* 4, 1742–1762. doi:10.1002/adhm.201500168

Du, X., Fu, S., and Zhu, Y. (2018). 3D printing of ceramic-based scaffolds for bone tissue engineering: an overview. *J. Mater. Chem. B* 6, 4397–4412. doi:10.1039/c8tb00677f

Einhorn, T. A., and Gerstenfeld, L. C. (2015). Fracture healing: mechanisms and interventions. *Nat. Rev. Rheumatol.* 11(1):45–54. doi:10.1038/nrrheum.2014.164

Elmowafy, E. M., Tiboni, M., and Soliman, M. E. (2019). Biocompatibility, biodegradation and biomedical applications of poly(lactic acid)/poly(lactic-co-glycolic acid) micro and nanoparticles. *J. Pharm. Investig.* 49, 347–380.

Erol, M., and Boccaccini, A. R. (2011). Nanoscaled bioactive glass particles and nanofibres. *Bioact. Glas.* 129–161. doi:10.1533/9780857093318.2.129

Felfel, R. M., Hossain, K. M. Z., Parsons, A. J., Rudd, C. D., and Ahmed, I. (2015). Accelerated *in vitro* degradation properties of polylactic acid/phosphate glass fibre composites. *J. Mater. Sci.* 50, 3942–3955. doi:10.1007/s10853-015-8946-8

Fiorilli, S., Molino, G., Pontremoli, C., Iviglia, G., Torre, E., Cassinelli, C., et al. (2018). The incorporation of strontium to improve bone-regeneration ability of mesoporous bioactive glasses. *Materials (Basel).* 11, 658. doi:10.3390/ma11050678

Fu, C., Bai, H., Zhu, J., Niu, Z., Wang, Y., Li, J., et al. (2017). Enhanced cell proliferation and osteogenic differentiation in electrospun PLGA/hydroxyapatite nanofibre scaffolds incorporated with graphene oxide. *PLoS One* 12, 1–20. doi:10.1371/journal.pone.0188352

Gentleman, E., Fredholm, Y. C., Jell, G., Lotfibakhshaiesh, N., O'Donnell, M. D., Hill, R. G., et al. (2010). The effects of strontium-substituted bioactive glasses on osteoblasts and osteoclasts *in vitro*. *Biomaterials* 31, 3949–3956. doi:10.1016/j.biomaterials.2010.01.121

Gibson, I., Rosen, D. W., and Stucker, B. (2010). *Additive manufacturing technologies*. New York, NY Springer.

Gilmer, E. L., Miller, D., Chatham, C. A., Zawaski, C., Fallon, J. J., Pekkanen, A., et al. (2018). Model analysis of feedstock behavior in fused filament fabrication: enabling rapid materials screening. *Polymer (Guildf).* 152, 51–61. doi:10.1016/j.polymer.2017.11.068

Jiang, Y., Yuan, Z., and Huang, J. (2019). Substituted hydroxyapatite: a recent development. *Mater. Technol.* 00, 1–12. doi:10.1080/10667857.2019.1664096

Kalani, M. M., Nourmohammadi, J., Negahdari, B., Rahimi, A., and Sell, S. A. (2019). Electrospun core-sheath poly(vinyl alcohol)/silk fibroin nanofibers with Rosuvastatin release functionality for enhancing osteogenesis of human adipose-derived stem cells. *Mater. Sci. Eng. C* 99, 129–139. doi:10.1016/j.msec.2019.01.100

Kalita, S. J., Bhardwaj, A., and Bhatt, H. A. (2007). Nanocrystalline calcium phosphate ceramics in biomedical engineering. *Mater. Sci. Eng. C* 27, 441–449. doi:10.1016/j.msec.2006.05.018

Kargozar, S., Fiume, E., Fiume, E., and Baino, F. (2019). Multiple and promising applications of strontium (Sr)-containing bioactive glasses in bone tissue engineering. *Front. Bioeng. Biotechnol.* 7. doi:10.3389/fbioe.2019.00161

Kasuga, T., Ota, Y., Nogami, M., and Abe, Y. (2000). Preparation and mechanical properties of polylactic acid composites containing hydroxyapatite fibers. *Biomaterials* 22, 19–23. doi:10.1016/S0142-9612(00)00091-0

Kaur, G., Pickrell, G., Kimsawatde, G., Homa, D., Allbee, H. A., and Sriranganathan, N. (2014). Synthesis, cytotoxicity, and hydroxyapatite formation in 27-Tris-SBF for sol-gel based CaO-P2O5-SiO2-B2O 3-ZnO bioactive glasses. *Sci. Rep.* 4, 1–14. doi:10.1038/srep04392

Kaygili, O., Keser, S., Kom, M., Eroksuz, Y., Dorozhkin, S. V., Ates, T., et al. (2015). Strontium substituted hydroxyapatites: synthesis and determination of their structural properties, *in vitro* and *in vivo* performance. *Mater. Sci. Eng. C* 55, 538–546. doi:10.1016/j.msec.2015.05.081

Kermani, F., Beidokhti, S. M., Baino, F., Gholamzadeh-Virany, Z., Mozafari, M., and Kargozar, S. (2020). Strontium-and cobalt-doped multicomponent mesoporous bioactive glasses (MBGS) for potential use in bone tissue engineering applications. *Materials (Basel).* 13, 1–20. doi:10.3390/ma13061348

Kumar, A., Kargozar, S., Baino, F., and Han, S. S. (2019). Additive manufacturing methods for producing hydroxyapatite and hydroxyapatite-based composite scaffolds: a review. *Front. Mater.* 6, 1–20. doi:10.3389/fmats.2019.00313

Lee, J., Lee, H., Cheon, K. H., Park, C., Jang, T. S., Kim, H. E., et al. (2019). Do Fabrication of poly(lactic acid)/Ti composite scaffolds with enhanced mechanical properties and biocompatibility via fused filament fabrication (FFF)–based 3D printing. *Addit. Manuf.* 30, 100883. doi:10.1016/j.addma.2019.100883

Lehmann, G., Cacciotti, I., Palmero, P., Montanaro, L., Bianco, A., Campagnolo, L., et al. (2012). Differentiation of osteoblast and osteoclast precursors on pure and silicon-substituted synthesized hydroxyapatites. *Biomed. Mater.* 7, 055001. doi:10.1088/1748-6041/7/5/055001

Liu, D., Nie, W., Li, D., Wang, W., Zheng, L., Zhang, J., et al. (2019). 3D printed PCL/SrHA scaffold for enhanced bone regeneration. *Chem. Eng. J.* 362, 269–279. doi:10.1016/j.cej.2019.01.015

Liu, X., Wang, T., Chow, L. C., Yang, M., and Mitchell, J. W. (2014). Effects of inorganic fillers on the thermal and mechanical properties of poly(lactic acid). *Int J Polym Sci.* 2014:827028. doi:10.1155/2014/827028

Melchels, F. P. W., Domingos, M. A. N., Klein, T. J., Malda, J., Bartolo, P. J., and Hutmacher, D. W. (2012). Additive manufacturing of tissues and organs. *Prog. Polym. Sci.* 37, 1079–1104. doi:10.1016/j.progpolymsci.2011.11.007

Melo, P., Ferreira, A. M., Waldron, K., Swift, T., Gentile, P., Magallanes, M., et al. (2019). Osteoinduction of 3D printed particulate and short-fibre reinforced composites produced using PLLA and apatite-wollastonite. *Compos. Sci. Technol.* 184, 107834. doi:10.1016/j.compscitech.2019.107834

Melo, P. (2019). Additive manufacturing of bioceramic and biocomposite devices for bone repair. PhD thesis. Tyne (England): Newcastle University

Melo, P., Tarrant, E., Swift, T., Townshend, A., German, M., Ferreira, A. M., et al. (2019). Short phosphate glass fiber - PLLA composite to promote bone mineralization. *Mater. Sci. Eng. C* 104, 109929. doi:10.1016/j.msec.2019.109929

Middleton, J. C., and Tipton, A. J. (2000). Synthetic biodegradable polymers as orthopedic devices. *Biomaterials* 21, 2335–2346. doi:10.1016/S0142-9612(00)00101-0

Narayanan, G., Vernekar, V. N., Kuyinu, E. L., and Laurencin, C. T. (2016). Poly (lactic acid)-based biomaterials for orthopaedic regenerative engineering. *Adv. Drug Deliv. Rev.* 107, 247–276. doi:10.1016/j.addr.2016.04.015

Navarro, M., Michiardi, A., Castaño, O., and Planell, J. A. (2008). Biomaterials in orthopaedics. *J. R. Soc. Interface* 5, 1137–1158. doi:10.1098/rsif.2008.0151

Neščáková, Z., Zheng, K., Liverani, L., Nawaz, Q., Galusková, D., Kaňková, H., et al. (2019). Multifunctional zinc ion doped sol – gel derived mesoporous bioactive glass nanoparticles for biomedical applications. *Bioact. Mater.* 4, 312–321. doi:10.1016/j.bioactmat.2019.10.002

Nienhaus, V., Smith, K., Spiehl, D., and Dörsam, E. (2019). Investigations on nozzle geometry in fused filament fabrication. *Addit. Manuf.* 28, 711–718. doi:10.1016/j.addma.2019.06.019

Ofudje, E. A., Adeogun, A. I., Idowu, M. A., and Kareem, S. O. (2019). Synthesis and characterization of Zn-Doped hydroxyapatite: scaffold application, antibacterial and bioactivity studies. *Heliyon* 5, e01716. doi:10.1016/j.heliyon.2019.e01716

Pisani, P., Renna, M. D., Conversano, F., Casciaro, E., Di Paola, M., Quarta, E., et al. (2016). Major osteoporotic fragility fractures: risk factor updates and societal impact. *World J. Orthop.* 7, 171–181. doi:10.5312/wjo.v7.i3.171

Pontiroli, L., Dadkhah, M., Novajra, G., Tcacencu, I., Fiorilli, S., and Vitale-Brovarone, C. (2017). An aerosol-spray-assisted approach to produce mesoporous bioactive glass microspheres under mild acidic aqueous conditions. *Mater. Lett.* 190, 111–114. doi:10.1016/j.matlet.2016.12.125

Qi, X., Wang, H., Zhang, Y., Pang, L., Xiao, W., Jia, W., et al. (2018). Mesoporous bioactive glass-coated 3D printed borosilicate bioactive glass scaffolds for improving repair of bone defects. *Int. J. Biol. Sci.* 14, 471–484. doi:10.7150/ijbs.23872

Querido, W., Rossi, A. L., and Farina, M. (2016). The effects of strontium on bone mineral: a review on current knowledge and microanalytical approaches. *Micron* 80, 122–134. doi:10.1016/j.micron.2015.10.006

Ramanath, H. S., Chua, C. K., Leong, K. F., and Shah, K. D. (2008). Melt flow behaviour of poly-ε-caprolactone in fused deposition modelling. *J. Mater. Sci. Mater. Med.* 19, 2541–2550. doi:10.1007/s10856-007-3203-6

Ramesh, N., Moratti, S. C., and Dias, G. J. (2018). Hydroxyapatite–polymer biocomposites for bone regeneration: a review of current trends. *J. Biomed. Mater. Res. - Part B Appl. Biomater.* 106, 2046–2057. doi:10.1002/jbm.b.33950

Sachlos, E., Czernuszka, J. T., Gogolewski, S., and Dalby, M. (2003). Making tissue engineering scaffolds work. Review on the application ofsolid freeform fabrication technology to the production of tissue engineeringscaffolds. *Eur. Cells Mater.* 5, 29–40. doi:10.22203/ecm.v005a03

Shikinami, Y., and Okuno, M. (2001). Bioresorbable devices made of forged composites of hydroxyapatite (HA) particles and poly L-lactide (PLLA). Part II: practical properties of miniscrews and miniplates. *Biomaterials* 22, 3197–3211. doi:10.1016/S0142-9612(01)00072-2

Thommes, M., Kaneko, K., Neimark, A. V., Olivier, J. P., Rodriguez-Reinoso, F., Rouquerol, J., et al. (2015). Physisorption of gases, with special reference to the evaluation of surface area and pore size distribution (IUPAC Technical Report). *Pure Appl. Chem.* 87, 1051–1069. doi:10.1515/pac-2014-1117

Tripathi, G., Choudhury, P., and Basu, B. (2010). Development of polymer based biocomposites: a review. *Mater. Technol.* 25, 158–176. doi:10.1179/175355510X12723642365089

Valino, A. D., Dizon, J. R. C., Espera, A. H., Chen, Q., Messman, J., and Advincula, R. C. (2019). Advances in 3D printing of thermoplastic polymer composites and nanocomposites. *Prog. Polym. Sci.* 98, 101162. doi:10.1016/j.progpolymsci.2019.101162

Wang, M. (2003). Developing bioactive composite materials for tissue replacement. *Biomaterials* 24, 2133–2151. doi:10.1016/S0142-9612(03)00037-1

Wang, X., Jiang, M., Zhou, Z., Gou, J., and Hui, D. (2017). 3D printing of polymer matrix composites: a review and prospective. *Compos. Part B Eng.* 110, 442–458. doi:10.1016/j.compositesb.2016.11.034

Wu, C., Chang, J., and Fan, W. (2012). Bioactive mesoporous calcium-silicate nanoparticles with excellent mineralization ability, osteostimulation, drug-delivery and antibacterial properties for filling apex roots of teeth. *J. Mater. Chem.* 22, 16801–16809. doi:10.1039/c2jm33387b

Wu, C., and Chang, J. (2012). Mesoporous bioactive glasses: structure characteristics, drug/growth factor delivery and bone regeneration application. *Interface Focus* 2, 292–306. doi:10.1098/rsfs.2011.0121

Xiao, G., Yin, H., Xu, W., and Lu, Y. (2016). Modification and cytocompatibility of biocomposited porous PLLA/HA-microspheres scaffolds. *J. Biomater. Sci. Polym. Ed.* 27, 1462–1475. doi:10.1080/09205063.2016.1211000

Xie, J., Blough, E. R., and Wang, C. H. (2012). Submicron bioactive glass tubes for bone tissue engineering. *Acta Biomater.* 8, 811–819. doi:10.1016/j.actbio.2011.09.009

Yan, X. X., Deng, H. X., Huang, X. H., Lu, G. Q., Qiao, S. Z., Zhao, D. Y., et al. (2005). Mesoporous bioactive glasses. I. Synthesis and structural characterization. *J. Non. Cryst. Solids* 351, 3209–3217. doi:10.1016/j.jnoncrysol.2005.08.024

Yan, X., Yu, C., Zhou, X., Tang, J., and Zhao, D. (2004). Highly ordered mesoporous bioactive glasses with superior *in vitro* bone-forming bioactivities. *Angew. Chemie - Int. Ed.* 43, 5980–5984. doi:10.1002/anie.200460598

Yilmaz, B., Alshemary, A. Z., and Evis, Z. (2019). Co-doped hydroxyapatites as potential materials for biomedical applications. *Microchem. J.* 144, 443–453. doi:10.1016/j.microc.2018.10.007

Yoon, S. D., Kwon, Y. S., and Lee, K. S. (2017). Biodegradation and biocompatibility of poly L-lactic acid implantable mesh. *Int. Neurourol. J.* 21, 48–54. doi:10.5213/inj.1734882.441

Yun, H. suk., Kim, S. H., Khang, D., Choi, J., Kim, H. hoon., and Kang, M. (2011). Biomimetic component coating on 3D scaffolds using high bioactivity of mesoporous bioactive ceramics. *Int. J. Nanomedicine* 6, 2521–2531. doi:10.2147/ijn.s25647

Zhao, S., Zhu, M., Zhang, J., Zhang, Y., Liu, Z., Zhu, Y., et al. (2014). Three dimensionally printed mesoporous bioactive glass and poly(3-hydroxybutyrate-co-3-hydroxyhexanoate) composite scaffolds for bone regeneration. *J. Mater. Chem. B* 2, 6106–6118. doi:10.1039/c4tb00838c

Zhu, H., Guo, D., Sun, L., Li, H., Hanaor, D. A. H., Schmidt, F., , et al.Xu, K. (2018). Nanostructural insights into the dissolution behavior of Sr-doped hydroxyapatite. *J. Eur. Ceram. Soc.* 38, 5554–5562. doi:10.1016/j.jeurceramsoc.2018.07.056

**Conflict of Interest:** Author AA and PQ were employed by the company FLUIDINOVA, S.A.

The remaining authors declare that the research was conducted in the absence of any commercial or financial relationships that could be construed as a potential conflict of interest.